Chapter

Fractal Geometry: An Attractive Choice for Miniaturized Planar Microwave Filter Design

Hadi T. Ziboon and Jawad K. Ali

Abstract

Various fractal geometries are characterized by the self-similarity and space-filling properties. The space-filling feature has been successfully applied to design multiband antenna structures for a wide variety of multifunction wireless systems. On another hand, the second feature has proved its validity to produce miniaturized antennas and passive microwave circuits including the band-pass filters (BPF). This chapter demonstrates the design of miniaturized microstrip BPFs that are derived from fractal-based DGS resonators. Many microstrip BPFs based on the Minkowski fractal DGS resonators will be presented together with those based on Moore and Peano fractal geometries. Simulation results, of all of the presented BPFs, show that an extra-size reduction can be obtained as the iteration level becomes higher. Measured and simulated results agree well with each other. A comparison has been conducted with other filters based on Peano and Hilbert fractal geometries. The results reveal that the proposed BPF offers acceptable performance and a significant decrease of higher harmonics.

Keywords: miniaturized microwave BPF, fractal-based DGS, Minkowski fractal geometry, Moore fractal geometry, Peano fractal geometry

1. Introduction

Microwave antenna and passive circuit designers have to meet the ever encountered challenges to produce components with miniaturized size and multiband operation. To meet these challenges, the various fractal geometries have been found to be an attractive choice. These geometries have two unique features: the space filling and the self-similarity. For more than two decades, these features have opened the novel and essential techniques for the design of the microwave antennas and passive circuits. The benefits of incorporating these geometries are, among many, enhanced bandwidths, compact sizes, partless electronic parts, and improved performance. Furthermore, fractal-based structures offer an additional epoch of optimizing design mechanisms. These mechanisms are applied successfully in the antenna design, although they can be implemented in a wide-ranging way [1].

Away from the application of the different fractals to produce small-size microwave filters, the use of fractal geometries has been earlier to take place. In this context, the antenna design and the distinctive features, that the various fractal-based structures have, were efficiently adopted to create compact size multi-resonant

antennas [2–9]. Besides, researchers have effectively proposed a variety of fractal geometries to modify to the typical microstrip structures which are efficiently endorsed to obtain miniaturized size of multiband antennas and BPFs for great types of wireless communication. In this perspective, the classical Euclidean shapes, such as the square, have been shaped in the form of the Sierpinski carpet to design a dual-mode BPF [10, 11]. Numerous traditional fractal structures attracted the microwave passive circuit designers to produce of miniaturized microstrip BPFs as well [12, 13]. Microstrip structures with Peano fractal-shaped resonators and its modification were employed in the conventional resonators to fabricate efficient miniaturized single- and dual-mode BPFs with single-band performance and also dual-mode implementation [14–17]. Researchers attempted to try modified versions of the classical fractals in the attempt to get higher space-filling curves to design highly miniaturized resonant structures. The modified variants of the Minkowski fractal proved its validity to suggest microstrip BPFs with more size reduction [18–21]. As an impressive result, the Minkowski fractal-based BPFs are characterized with a resonant performance with reduced harmonics [22].

In contrast, the defected ground structures have been applied to design miniaturized BPFs. Enhanced filter characteristics have shown to be attractive, and a growing research effort has been devoted to this topic as implied in the literature. However, most of the reported studies have been dedicated to the design of the microstrip LPFs. It is worth here to say that the application of various fractals and their variants to reshape the defected ground structures has revealed to be successful to offer extra-size reduction besides the improved filter performance [23–28]. The conventional Hilbert fractal geometry has been adopted to modify a defected ground structure in an attempt to produce a miniaturized microstrip low-pass filter [23]. A defected ground structure that has been modeled according to the Hilbert fractal curve is implemented to enhance the out-of-band performance of the filter. The fractal structure has been loaded with open stubs for this purpose. The Sierpinski carpet-based defected ground structure is successfully utilized to produce a microstrip low-pass filter as reported in [24]. Also, the variants of the Minkowski and Koch fractals were employed to modify the shape of a defected ground structure CSRR to produce a compact-size band-pass filter [25, 26].

In this chapter, the design of a miniaturized microstrip band-pass filter is loaded with a fractal-shaped defected ground structure. A Minkowski fractal variant, with various iteration orders, has been adopted in the modification of the form of the defected ground structure of the proposed BPF. In addition to the reduced size, the proposed band-pass filter is found to present acceptable resonant characteristics with harmonics reduction capability. Even though the various fractals in the production of defected ground structure resonators are used to construct miniaturized microstrip band-pass filters, it is interesting to mention that the proposed filter design presented in this work has overperformed numerous of its category since it possesses a considerably reduced size besides the acceptable performance.

2. The modified Minkowski fractal geometry

The most critical criterion in the selection of a fractal curve, from the aspect of the microwave circuit miniaturization, is its dimension. The higher the fractal dimension, the better the fractal curve fills the given area, therefore achieving higher compactness. The generation process of the traditional Minkowski fractal curve is adopting a square with 1/3 unit side length, instead of an equilateral triangle of the same side length. The corresponding fractal dimension is 1.465. For comparison purposes, **Table 1** shows the fractal dimensions of some fractal curves

Fractal curve type	Fractal dimensions
Koch curve	1.2618
Sierpinski triangle	1.5848
Sierpinski carpet	1.8928
Koch snowflake	1.2618
Cantor set	0.631
Minkowski curve	1.465

Table 1.
The fractal dimensions of some fractal geometries [29].

that are widely adopted in the design of microwave antennas and circuits. For this, to enhance the input/output coupling and to obtain a practical range of the fractal dimension of the standard Minkowski fractal curve, a modified variant is introduced.

Figure 1 illustrates the generation process of the proposed Minkowski fractal variant. The figure shows the generation of the modified version up to the second iteration as applied to a square ring. In this version, the typical 1/3 ratio which is the most popular in the generation of the majority of various fractal curves has been replaced by an arbitrary ratio.

As the generation process implies, the shape variations in the sequential steps, depicted in **Figure 1(b)–(d)**, can be thought as a means to enlarge the surface charge density pat as compared with that of the typical square ring resonator. This increase of the path length will lead to lower the resonant frequency. In other words, this will decrease the size of the resulting filter if the operating frequency is kept unchanged. For the nth iteration, the proposed Minkowski fractal variant has been found to have the perimeters given by

$$P_n = \left(1 + 2\frac{w_2}{L_o}\right) P_{n-1} \tag{1}$$

where P_n is the perimeter of the nth iteration fractal structure, w_2 and L_o are as depicted in **Figure 1**. Examining Eq. (1) and **Figure 1**, it is clear that at a specific iteration level, when varying w_1, w_2, or both, a broad diversity of structures with distinctive perimeters can be achieved.

According to Falconer [29], the modified version of the Minkowski fractal geometry is called multi-fractal or fractal geometry with more than one ratio in the generator: a_1 and a_2. For this case, the fractal dimension, D, can be obtained from the solution of the following equation:

$$2\left(\frac{1}{2}(1 - a_1)\right)^D + 2a_2^D + a_1^D = 1 \tag{2}$$

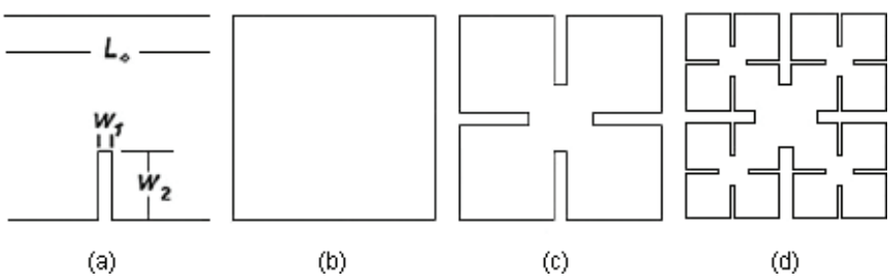

Figure 1.
The generation process of the proposed Minkowski fractal variant [18, 25].

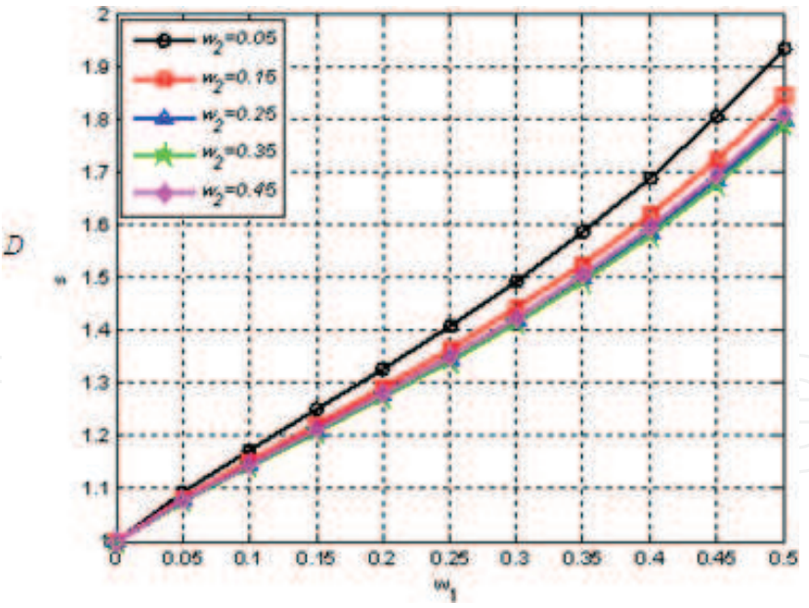

Figure 2.
The variation of the fractal dimensions of the modified Minkowski fractal with the parameter w_2 as a parameter [30].

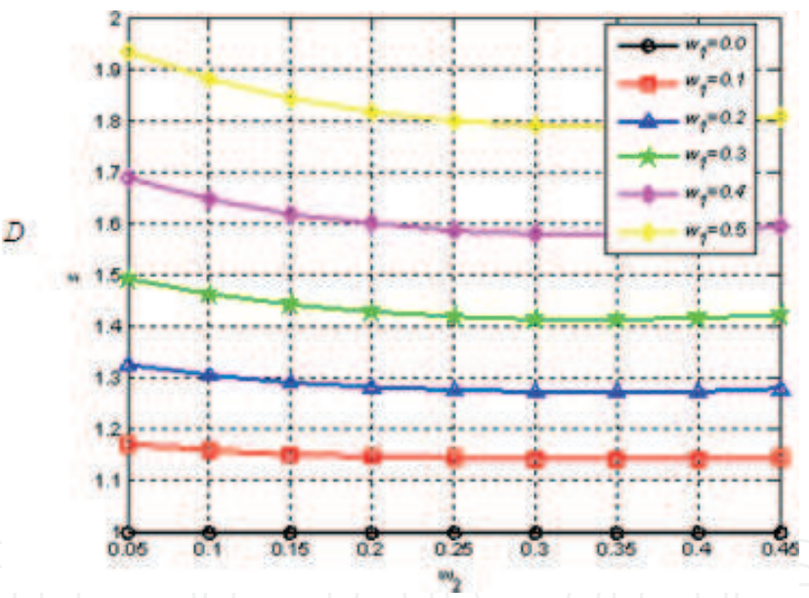

Figure 3.
The variation of the fractal dimensions of the modified Minkowski fractal with the parameter w_1 as a parameter [30].

where a_1 and a_2 are the ratios w_1/L_o and w_2/L_o, respectively. The parameters w_1, w_2, and L_o are as indicated in **Figure 1**.

To demonstrate the effects of varying w_1 and w_2 on the resulting dimension of the modified Minkowski fractal structure, Eq. (2) has been plotted against w_1 and w_2 for as shown in **Figures 2** and **3**, respectively. The parameter w_1 has been varied from zero to 0.5 in steps 0.1, while w_2 has been ranged from 0.05 to 0.45 in steps of 0.1.

Examining **Figures 1–3** and Eq. (2), it is clear that when w_1 is equal to zero, the fractal dimension will equal to 1, which represents the non-fractal state. In this case, the resulting structure is not with a fractal shape; it is merely a Euclidean square which has the dimension of 1. Furthermore, when w_1 and w_2 are both equal to 1/3, which is the case with the conventional Minkowski fractal curve, the dimension will be 1.465 as shown in **Table 1**.

As a conclusion, it is likely that further size reduction will take place after the application of the fractal-based structures to the traditional Euclidean-shaped resonators. This process implies that the increased space filling of the modified structures, at the successive iteration levels, will lead to an additional size reduction. The enlargement in the resulting length will result in the reduction of the corresponding size required to implement the fractal-based BPF. Hypothetically, as n goes to infinity, the resulting occupied length will approach to infinity. The capability of the new structure to enlarge its length in the following iteration levels has been shown fascinating for investigating its size reduction ability as a microstrip BPF.

3. The proposed filter design

In this work, many band-pass filters with fractal-based defected ground structures were modeled. The ground planes of these microstrip filters are defected using slots in the shape of two coupled resonators [31]. The suggested DGS consists of two coupled open-loop slot resonators in the form of the Minkowski fractal variants depicted in **Figure 1(b)–(d)**. Three microstrip band-pass filters have been modeled. Each filter has a fractal-based defected ground structure corresponding to a specified iteration order. The performance evaluation of each filter has been carried out using the commercially available EM simulator, IE3D [32].

Figure 4 demonstrates the configuration of the proposed microstrip DGS BPF filter. Here, it is clear that L denotes the resonator side lengths of the filters, D is the gap width, X is the inter-resonator spacing, and W is the distance between the longitudinal filter center and the transmission line lower edge. It is apparent that two coupled open-loop slots defect the ground plane of this filter. The slots take the shape of the Minkowski fractal variant of the second iteration. The proposed band-pass filter is constructed using a substrate with a relative permittivity of 2.65 and thickness of 1.0 mm. A microstrip transmission line is printed on the top of the substrate as shown in **Figure 4(b)**. A gap with a width D is etched in its center.

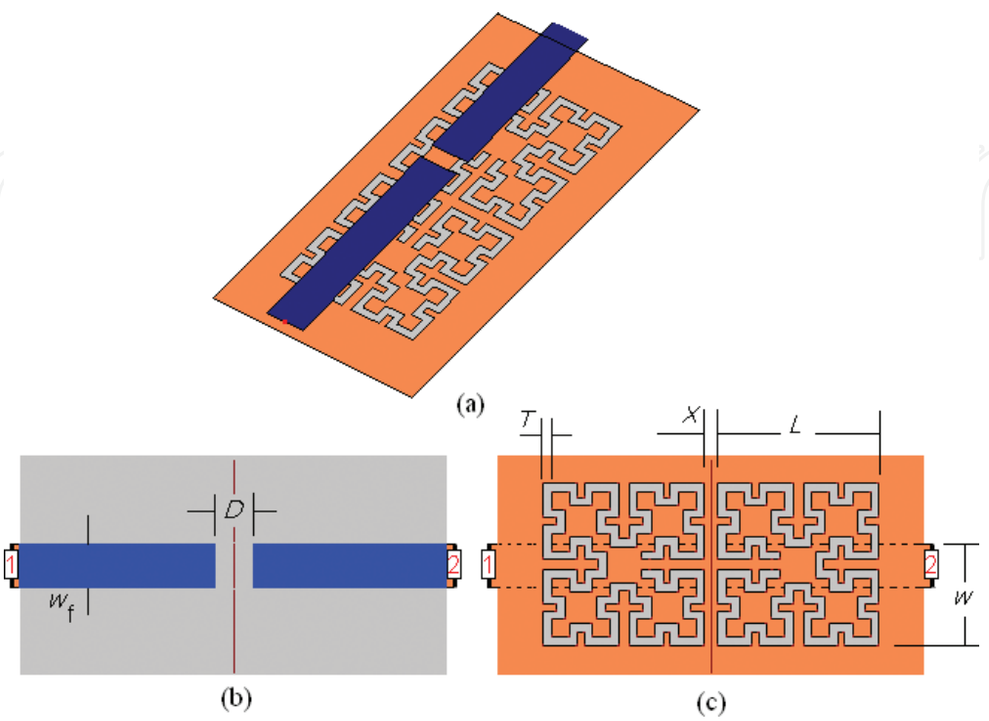

Figure 4.
(a) The layout of the proposed DGS BPF, (b) the front and (c) the back views [31].

The input/output ports have 50 Ω characteristic impedance. The corresponding transmission line width is found to be 2.75 mm. The defected ground structures are etched on the bottom side of the substrate as demonstrated in **Figure 4(c)**.

Throughout the simulation of the proposed BPF, the length L is maintained constant as that of the open-square-loop resonator. Consequently, at the design frequency of 2.45 GHz, the length L, for the simulated band-pass filter with the square open-loop resonator is equal to 12.50 mm at resonance. This value corresponds to about 0.15 λ_g. Then, λ_g is calculated as

$$\lambda_g = \frac{\lambda_o}{\sqrt{\varepsilon_{reff}}} \tag{3}$$

where ε_{eff} is the effective permittivity. Various EM simulators provide the means to calculate ε_{eff} using an embedded calculator. However, the empirical expressions required for the computation of ε_{eff} can be found in the literature [33]. On the other hand, the application of the fractal structures means that an extensive length will be added to that of the resonator structures. In this case, it is not conditional that the new lengths are equal to half or multiple of λ_g at resonance. This is because not all the resonator length will be part of the cause of realizing resonance. This fact becomes more evident when studying the charge density distributions on the various parts of the modeled filters.

It should be mentioned that the resonator lengths, L, of the simulated BPFs are kept fixed at a specified value. In the next section, it will become apparent that the parameters D, X, and W play a crucial influence on the final BPF resonant responses.

4. The simulation results

The resonant response of a band-pass filter is, in general, assessed all over its passband specifications, together with its passband insertion loss. It is essential that the insertion loss has not exceeded a certain specified level, and it should be reliably below some particular value throughout the occupied passband. The band-pass filter has to offer as much elimination of undesired signals as possible, both in its lower stopband and upper stopband outside of the low-loss passband. However, to describe the degree of selectivity of a band-pass filter, the term what is the roll-off rate is introduced [34, 35]. The roll-off rate, R, of a BPF response, is defined as

$$R = \frac{|\alpha_{max} - \alpha_{min}|}{|f_s - f_c|} \tag{4}$$

where α_{max} and α_{min} are the 40 dB and the 3 dB attenuation points, respectively, while f_s and f_c are the 40 dB stopband and the 3 dB cutoff frequencies. It should

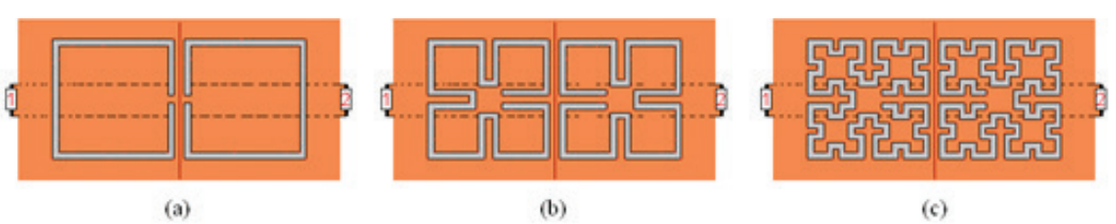

Figure 5.
The configurations of the simulated band-pass filters with: (a) zero, (b) first iteration, and (c) the second iteration fractal-based defected ground structures [31].

be noted that various values might be specified for α_{max} to find out the roll-off rate [36]. However, in this work α_{max} has been chosen to be 40 dB. Many BPFs with the defected ground structures, based on those shown in **Figure 5**, were modeled, and their performance responses have been evaluated. Two BPFs were modeled, both with the fractal-based resonators defected ground structures as those shown in **Figure 5(a)** and **(b)**.

5. A parametric study

Three band-pass filters with fractal-detected ground structures, shown in **Figure 5(a)–(c)**, were simulated, and their performance responses have been evaluated. The side length L of all the coupled DGS resonators of the modeled filters has been kept unchanged at 12.50 mm and slot trace width, T of about 0.61 mm. At this length, the zero iteration-detected ground structure BPF resonates at 2.50 GHz. For the three modeled filters, a parametric study was achieved to explore the effects of the different BPF elements, mainly D, X, and W, on its resonant behavior as will be presented in the following subsections.

5.1 The first iteration fractal DGS BPF

The impact of making the gap width D varied, while maintaining the other filter structure elements fixed, has been demonstrated in **Figure 6**. The increment of D causes the response transmission zeros to move away from the center frequency position, while approximately it does not affect the filter passband. Furthermore, as D is increased further, the realized BPF bandwidth is extended at the expense of the reduction of the filter selectivity. At a specific value of D, the upper transmission zero will vanish.

On the other hand, when the spacing X is made variable, the resulting responses are displayed in **Figure 7**. In contrast with the impact of changing D, the variation of X will be insignificant on the overall filter response including both the passband and the stopband.

The variation of the distance between the longitudinal filter center and the transmission line lower edge, W, has a considerable impact on the resulting filter responses as clearly demonstrated in **Figure 8**. In this case, both of the filter passband and stopband are significantly worsened. As the feed line becomes near the edge of

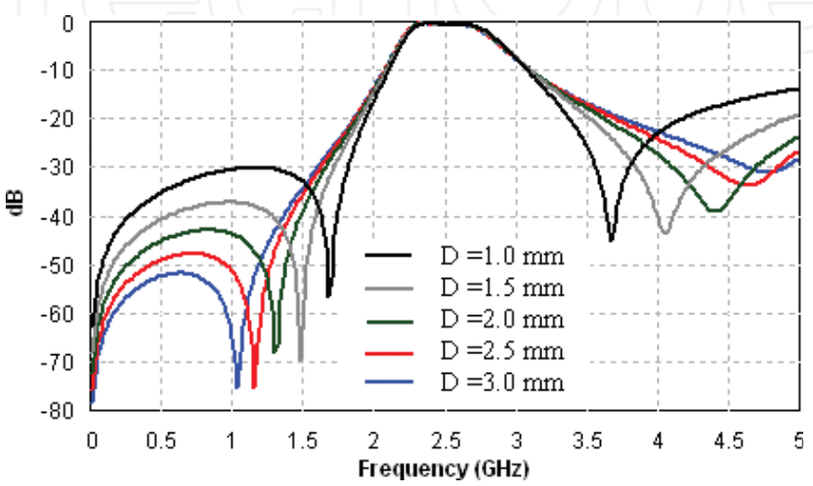

Figure 6.
The simulated scattering coefficient S_{21} responses of the modeled DGS BPF depicted in Figure 5(a) with the gap width, D, as a parameter.

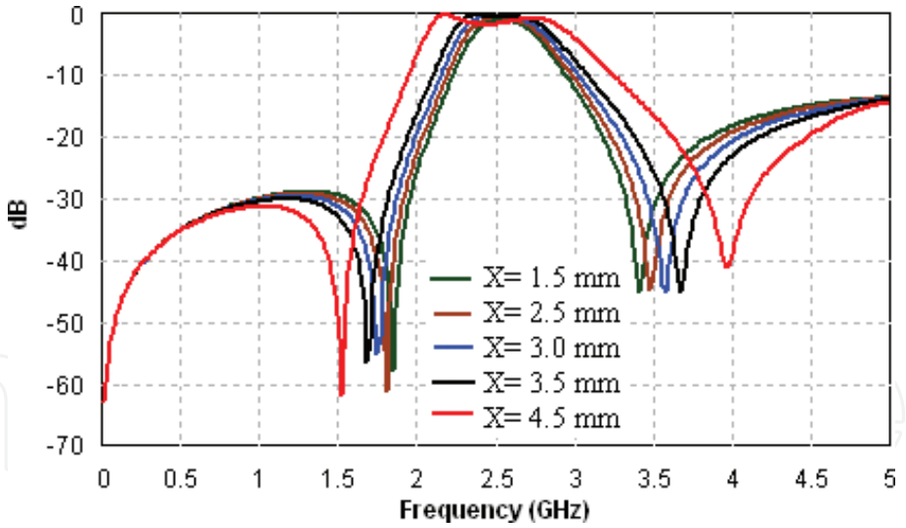

Figure 7.
The simulated scattering coefficient S_{21} responses of the modeled DGS BPF depicted in Figure 5(a) with the inter-resonator spacing, X, as a parameter.

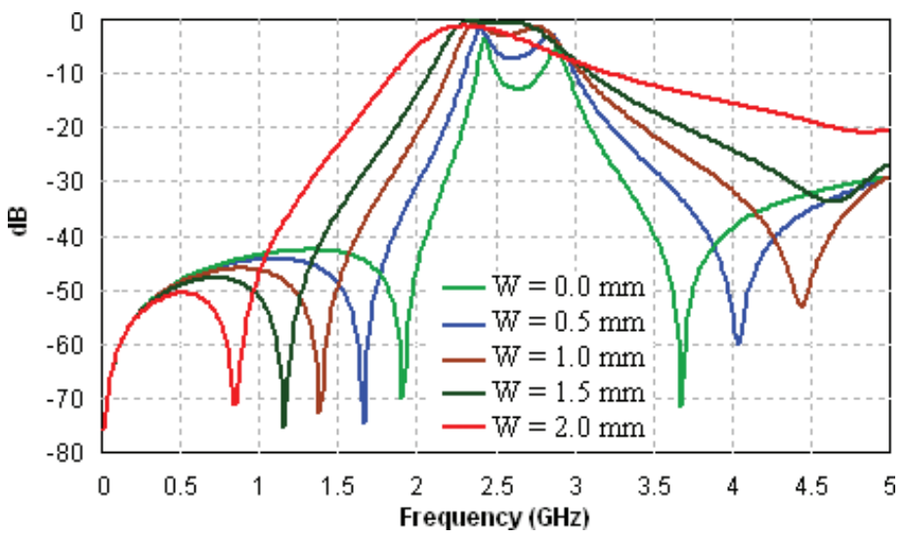

Figure 8.
The simulated scattering coefficient S_{21} responses of the modeled DGS BPF depicted in Figure 5(a) with the distance between the longitudinal filter center and the transmission line lower edge, W, as a parameter.

the defected ground structure, an improvement of the resonant filter responses will take place. Best performance has found at W = 1.5 mm, X = 2.5 mm, and D = 1.0 mm.

5.2 The first iteration fractal DGS BPF

An analogous investigation is performed to explore the effects of the parameters D, X, and W of this filter on its performance.

In this study, the side length of the fractal-based defected ground structure of this filter is kept the same as in Section 5.1. The additional length, that is made available by the application of the first iteration fractal resonator, causes the resulting BPF to resonate at a lower frequency. The S_{21} responses imply that this BPF resonates at 1.61 GHz. A comparison of the DGS BPF responses, those of this filter, reveals that this filter offers a size reduction of about 65%.

In addition to the size miniaturization offered by this filter, the resonant responses show that it overperforms that with the conventional DGS. This filter

provides an improved selectivity. The impacts of the modification of the parameters D, X, and W on the filter S_{21} responses are correspondingly demonstrated in **Figures 9–11**.

In summary, the resonant responses shown in **Figures 9–11** imply that this filter offers a most favorable resonant performance when the parameters W = 2.25 mm, X = 2.0 mm, and D = 0.25 mm. This filter provides a resonant response with a center frequency of 1.61 GHz. The resonant response is symmetrical about the center frequency. The results also reveal that the filter resonant response shows two transmission zeros located at 1.33 and 2.15 GHz. Furthermore, the resonant filter behavior is characterized by a steeper response with higher roll-off rates of 132.74 and 94.81 dB/GHz, at the lower and the upper edges of the passband, respectively. More interesting, this BPF provides an extra rejection level in the stopband when compared with that offered by the filter depicted in Section 5.1.

5.3 The second iteration fractal DGS BPF

The resonant behavior of this filter has also been studied under the impacts of varying the same parameters on its overall performance.

In this context, it has been that this filter possesses the optimal performance among those examined in Sections 5.1 and 5.2. The filter scattering coefficient, S_{21}, responses under the influence of the variation of the parameters D, X, and W are demonstrated in **Figures 12–14**, respectively. It is apparent from these responses that this band-pass filter overperforms the other two BPFs in several aspects that this filter presents the maximum selectivity and the top rejection level in the stopband.

Examining the resonant characteristics of this filter, it has an exciting performance with a steep roll-off in its in-band response. The –40 dB lower edge roll-off rate of the passband is of 197.70 dB/GHz and that of the upper edge is of 180.04 dB/GHz. Also, the resonant response shows that it has two transmission zeros almost symmetrically positioned about the center frequency. These transmission zeros are placed at 1.32 and 1.87 GHz. More interestingly, the filter performance responses reveal that it does not support the higher harmonics. Besides, according to [27, 28], the locations of the transmission zeros, in the filter response, are immensely influenced by the equivalent capacitance of the defected ground structures. Consequently, the improvement of the selectivity of this filter can be clarified as follows. When applying iteration levels, the incorporated length will become

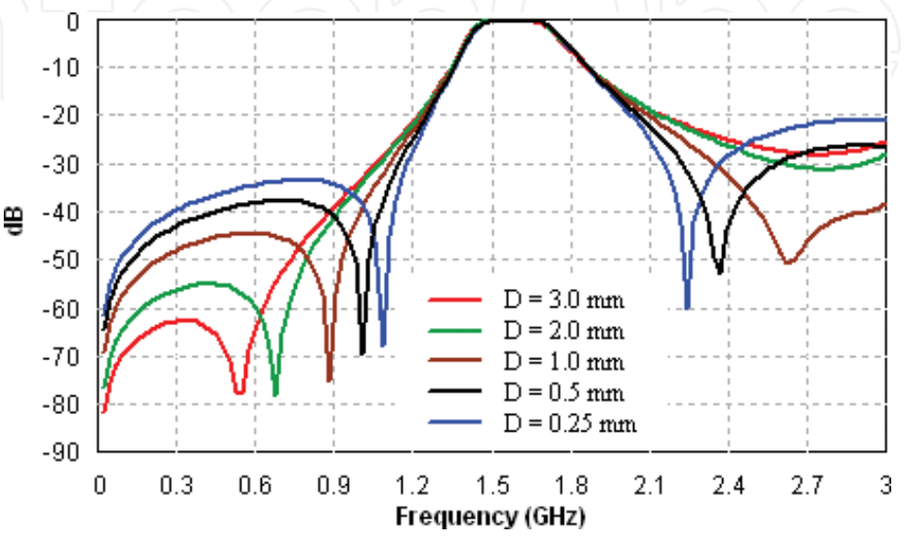

Figure 9.
The simulated scattering coefficient S_{21} responses of the modeled DGS BPF depicted in Figure 5(b) with the gap width, D, as a parameter.

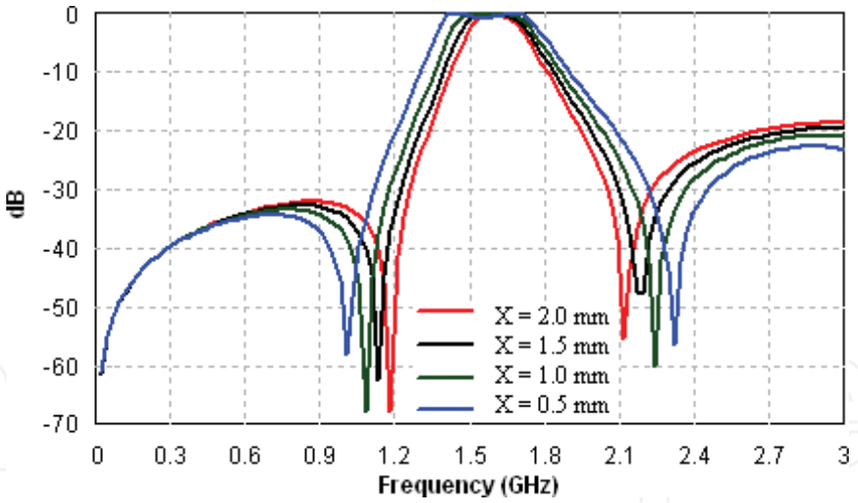

Figure 10.
The simulated scattering coefficient S_{21} responses of the modeled DGS BPF depicted in Figure 5(b) with the inter-resonator spacing, X, as a parameter.

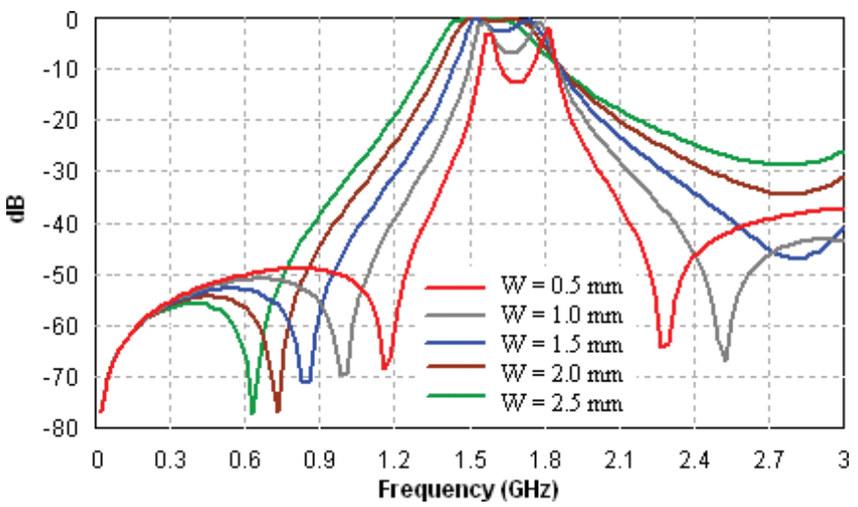

Figure 11.
The simulated scattering coefficient S_{21} responses of the modeled DGS BPF depicted in Figure 5(b) with the distance between the longitudinal filter center and the transmission line lower edge, W, as a parameter.

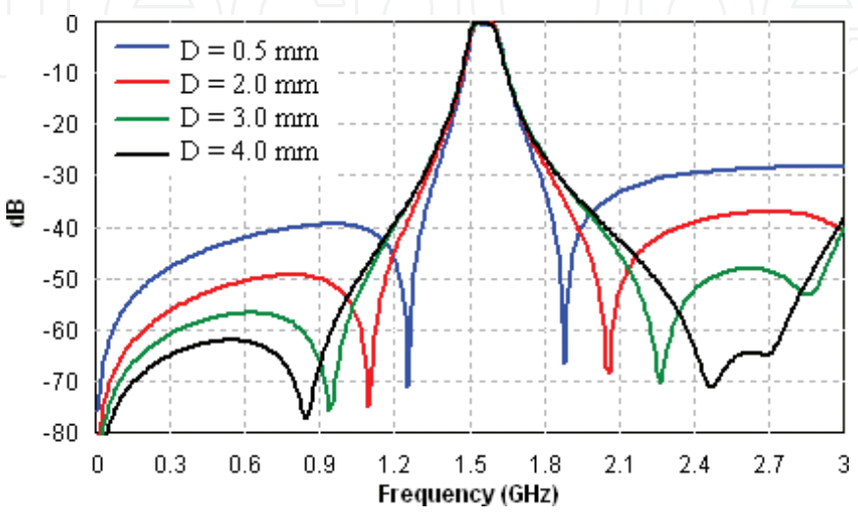

Figure 12.
The simulated scattering coefficient S_{21} responses of the modeled DGS BPF depicted in Figure 5(c) with the gap width, D, as a parameter.

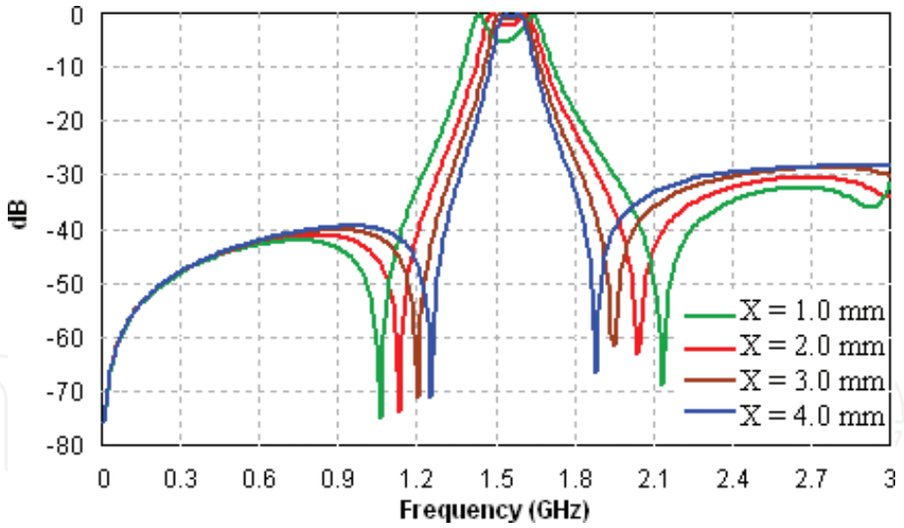

Figure 13.
The simulated scattering coefficient S_{21} responses of the modeled DGS BPF depicted in Figure 5(c) with the inter-resonator spacing, X, as a parameter.

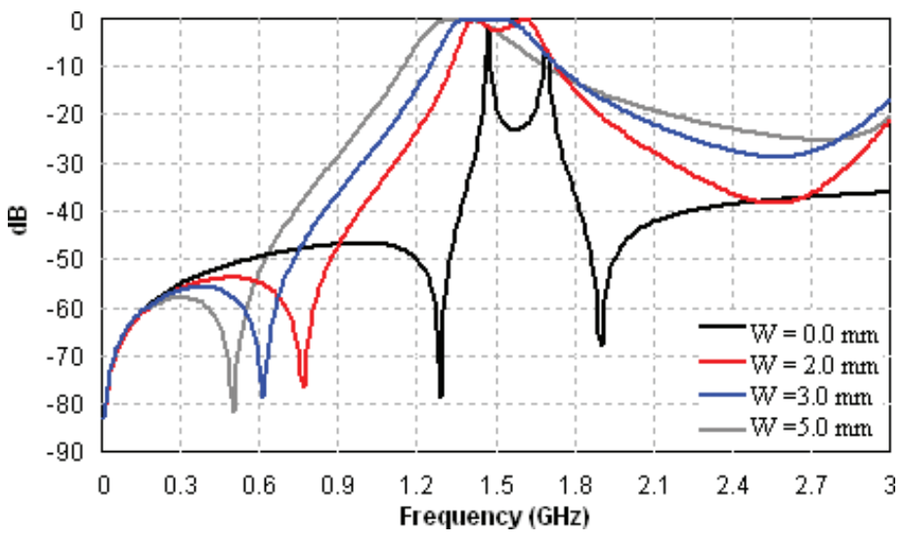

Figure 14.
The simulated scattering coefficient S_{21} responses of the modeled DGS BPF depicted in Figure 5(c) with the distance between the longitudinal filter center and the transmission line lower edge, W, as a parameter.

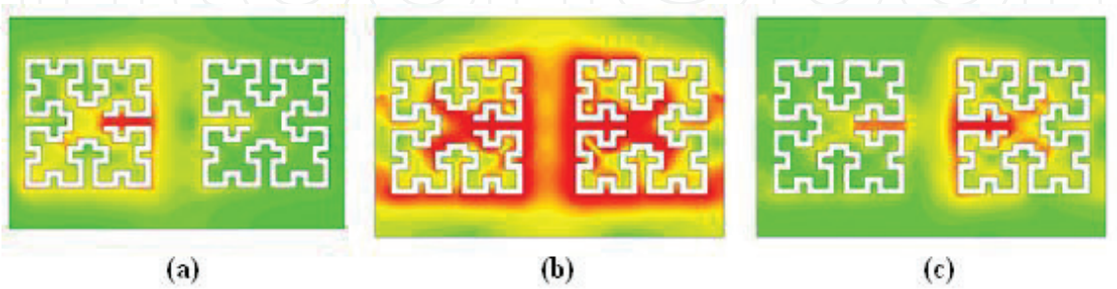

Figure 15.
The current distributions on the surface of the ground plane of the filter at different frequencies in the resonant band and outside it.

larger. The resulting substructures of the fractal-based resonators approach each other, leading to the existence of a capacitive coupling which, in turns, enhances the final filter skirt characteristics at both sides.

What is more, to offering an additional physical clarification about the electromagnetic aspects of the modeled band-pass filter, the current distributions on its surface have been simulated at different frequencies in the resonant band and outside it. **Figure 15(a)–(c)** illustrate the surface current distributions at 1.30, 1.55, and 1.70 GHz which represent the frequencies in the lower stopband, in the passband, and in the upper stopband, respectively. **Figure 15** exhibits the current distributions on the surfaces of the ground plane of the modeled BPF structure. **Figure 15(a)** and **(c)** indicates that there is no coupling taking place between the resonators in the lower stopband and the upper stopband. On the other hand, the large current densities, exposed in **Figure 15(b)**, represent an indication of the strong coupling which results in the conclusive resonance. It is apparent that the majority of the resonator length plays a role in causing the resonance.

6. Comparison with other fractal-based filter models

In this chapter, the modified Minkowski fractal geometry has been adopted to design the proposed BPF filter. The modified Minkowski fractal geometry is with better space-filling property to achieve more miniaturization as compared with the conventional Minkowski fractal geometry. However, an attempt has been carried out to compare the performance of the proposed filter with those modeled using other fractal geometries with high space-filling properties.

For this purpose, Peano and Moore fractal geometries have been adopted to design two BPFs based on the presented design idea. In the modeling of the proposed BPF filters, the same substrate and the same resonator dimensions are used. **Figures 16** and **17** illustrate the filter structures together with their performance

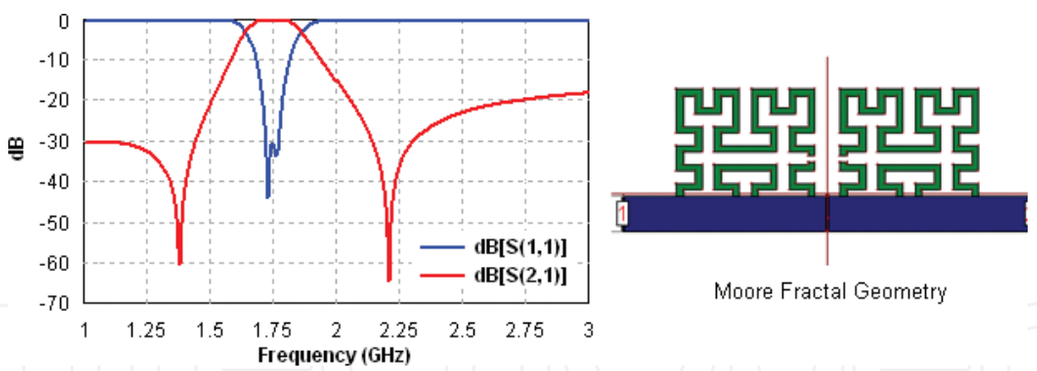

Figure 16.
Moore fractal-based DGS BPFs together with performance responses.

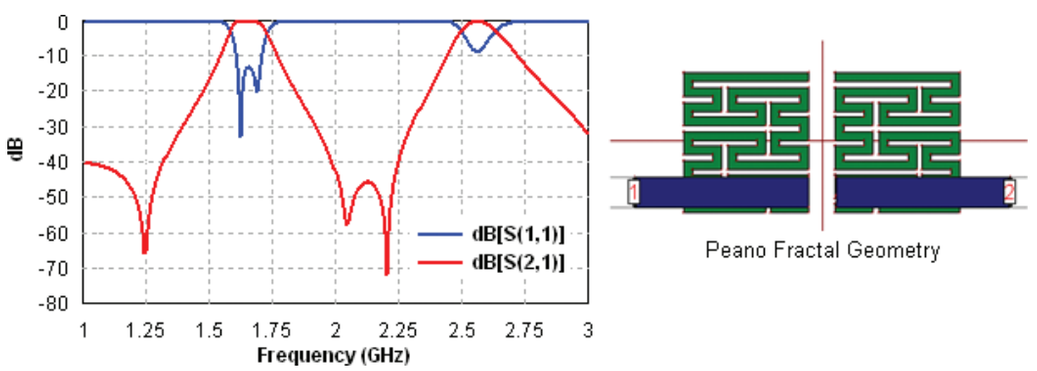

Figure 17.
Peano fractal-based DGS BPFs together with performance responses.

responses. It is clear that both filters offer resonant responses at a higher frequency than that provided by the Minkowski fractal-based BPF. This means that the Minkowski fractal-based BPF possesses a higher size reduction. It is worth to note that the BPF based on Peano fractal geometry offers dual-band resonant response which can be tuned to a certain extent by the filter elements. However, further investigation of this filter has to be conducted later.

7. Fabricated model and the measured results

A prototype of the fractal-based defected ground structure band-pass filter has been manufactured. The fabricated prototype uses an identical substrate with a relative permittivity of 2.65 and thickness of 1.0 mm. **Figure 18** shows photos of the manufactured filter. The measured and simulated scattering coefficient responses, S_{11} and S_{21}, are depicted in **Figures 19** and **20**, respectively.

The simulated and measured results of the modeled and the fabricated band-pass filters well agree with each other. Some deviation, between the measured and the simulated results, is noticed. The shift of the lower edge of the passband response of the S_{21} responses is slight, while that of the upper edge is hardly visible. Furthermore, the measured results reveal attenuation in the passband region.

The production technique might cause dimensional tolerance which, in turns, leads to the differences observed between the measured and the simulated results. Employing more advanced manufacturing methods, besides the selection of a substrate having a more stable parameter, will result in a closer agreement.

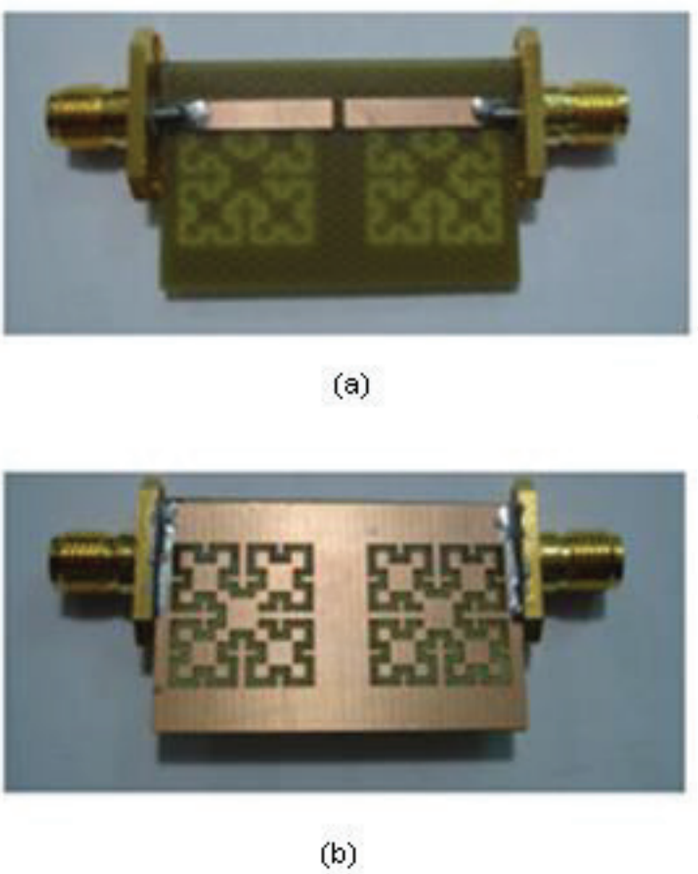

Figure 18.
Photos of the fabricated prototype (a) the top and (b) the bottom views.

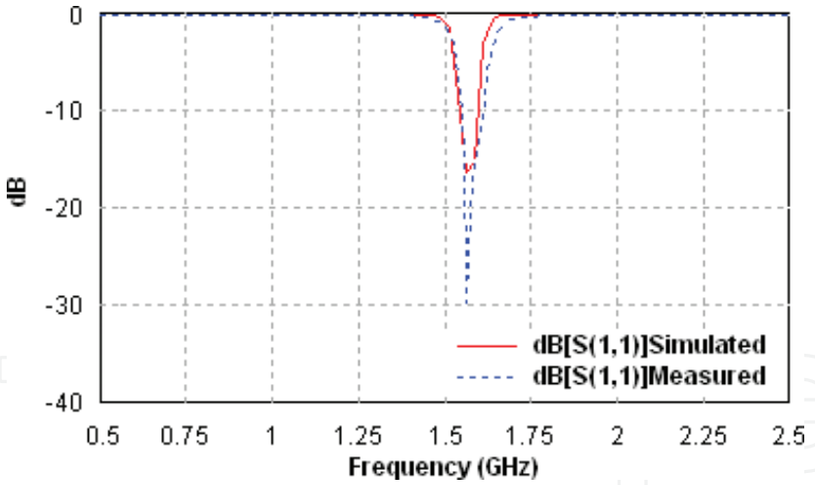

Figure 19.
The simulated and measured S_{11} responses of the fabricated filter prototype.

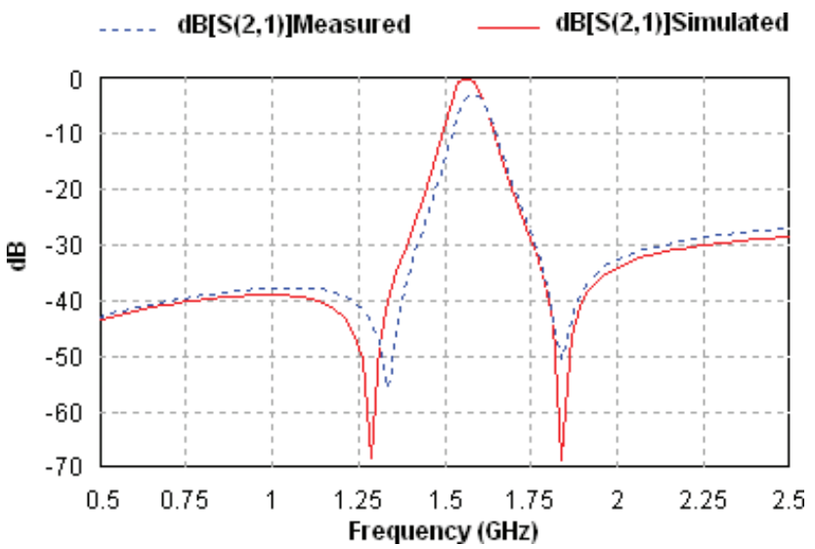

Figure 20.
The simulated and measured S_{21} responses of the fabricated filter prototype.

The resonant behaviors of the modeled band-pass filters suggested in this work have to be compared with those recently reported in the literature. **Table 2** summarizes a comparison of the performances of the presented filters which are based on the zero, first, and second iteration DGS band-pass filters with those recently reported in the literature [27, 28]. As the table implies, the comparison is carried out

Filter type	Filter size $[\lambda_g]^2$	Roll-off rate (lower edge) (dB/GHz)	Roll-off rate (upper edge) (dB/GHz)
Zero iteration DGS	0.45 × 0.23	78.51	47.10
First iteration DGS	0.30 × 0.15	132.74	94.81
Second iteration DGS	0.29 × 0.14	197.70	180.04
DGS BPF [27]	0.50 × 0.25	72.54	52.86
DGS BPF [28]	0.22 × 0.17	41.11	12.75

Table 2.
Comparison of the presented band-pass filters with those published in the literature.

concerning the occupied areas and the filter selectivity which in turns is expressed by the roll-off rates at the lower and the upper edges. In spite of the extra miniaturization of the second iteration, fractal-based DGS band-pass filter is minor, but this BPF possesses the most excellent selectivity, among the others, regarding the lower and the upper edges roll-off rates. However, the realized size by each BPF has been calculated in terms of the guided wavelength, λ_g, computed at the lower resonant frequency. Even though the DGS band-pass filter reported in [28] is approximately equivalent in the occupied area with that suggested in this work, it suffers from poor selectivity. It has poor upper edge roll-off rate and low selectivity in the lower edge roll-off rate.

8. Conclusions

The defected ground structure resonator based on the Minkowski fractal variant reported in this chapter has confirmed its capability to produce reduced size microstrip band-pass filters. Besides the acceptable resonant responses of the suggested BPFs, the adoption of the Minkowski fractal geometry to the defected ground structure resonator bring about BPF designs with considerable miniaturization with reference to those recently published in the literature. As expected, the results showed that more filter size miniaturization could be obtained when employing higher fractal orders. In the real practice, this might not be the situation; several restrictions are coming across the practical implementation of a filter prototype, especially for the higher iteration levels. Also, the results revealed that the proposed BPF performances are characterized by a low loss in the passband and high rejection in the stopband with considerable reduction of higher harmonics. A significant finding is that the final BPF performance possesses a high selectivity with steep roll-off rates at both the lower and the upper edges of the passband. A comparison of the performance of the DGS BPF based on the modified Minkowski fractal geometry with other filters based on Peano and Hilbert fractal geometries revealed that the proposed BPF has acceptable resonant responses with a significant lessening of higher harmonics. Measured results of a fabricated prototype well agree with those evaluated by the EM simulator. The presented BPF resonant characteristics, besides the considerable size miniaturization, will make it an appropriate candidate for the application in a broad diversity of the modern wireless communication services.

Conflict of interest

The authors declare there are no conflicts of interest regarding the publication of this book chapter.

Author details

Hadi T. Ziboon and Jawad K. Ali*
Microwave Research Group, Department of Electrical Engineering, University of Technology, Iraq

*Address all correspondence to: jawadkali@theiet.org

IntechOpen

References

[1] Cohen N. Fractal antenna and fractal resonator primer. Chapter 8. In: Rock JA, van Frankenhuijsen M, editors. Fractals and Dynamics in Mathematics, Science, and the Arts: Theory and Applications. Vol. 1. World Scientific Publishing, USA; 2015

[2] Ali JK, Ahmed ES. A new fractal based printed slot antenna for dual band wireless communication applications. In: Proceedings of Progress in Electromagnetics Research Symposium, PIERS 2012; Kuala Lumpur, Malaysia; 2012. pp. 1518-1521

[3] Ali JK, Jalal ASA. A miniaturized multiband Minkowski-like pre-fractal patch antenna for GPS and 3g IMT-2000 Handsets. Asian Journal of Information Technology. 2007;**6**(5):584-588

[4] Ali JK, Yassen MT, Hussan MR, Salim AJ. A printed fractal based slot antenna for multi-band wireless communication applications. In: Proceedings of Progress in Electromagnetics Research Symposium, PIERS 2012; Moscow, Russia; 2012. pp. 618-622

[5] Mezaal YS. New compact microstrip patch antennas: Design and simulation results. Indian Journal of Science and Technology. 2016;**9**(12):1-6. DOI: 10.17485/ijst/2016/v9i12/85950

[6] Abdulkarim SF, Salim AJ, Ali JK, Hammoodi AI, Yassen MT, Hussan MR. A compact Peano-type fractal based printed slot antenna for dual-band wireless applications. In: 2013 IEEE International RF and Microwave Conference, RFM 2013; Penang, Malaysia; 2013. pp. 329-332

[7] Ali JK, AL-Hussain ZAA, Osman AA, Salim AJ. A new compact size fractal based microstrip slot antenna for GPS applications. In: Proceedings of Progress in Electromagnetics Research Symposium, PIERS 2012; Kuala Lumpur, Malaysia; 2012. pp. 700-703

[8] Ali JK, Abdulkareem SF, Hammoodi AI, Salim AJ, Yassen MT, Hussan MR, et al. Cantor fractal based printed slot antenna for dual band wireless applications. International Journal of Microwave and Wireless Technologies. 2016;**8**(02):263-270

[9] Ghiyasvand M, Bakhtiari A, Sadeghzadeh RA. Novel microstrip patch antenna to use in 2×2 sub arrays for DBS reception. Indian Journal of Science and Technology. 2012;**5**(7):2967-2971. DOI: 10.17485/ijst/2012/v5i7/30493

[10] Ye CS, Su YK, Weng MH, Wu HW. Resonant properties of the Sierpinski-based fractal resonator and its application on low-loss miniaturized dual-mode bandpass filter. Microwave and Optical Technology Letters. 2009;**51**:1358-1361

[11] Weng MH, Jang LS, Chen WY. A Sierpinski-based resonator applied for low loss and miniaturized bandpass filters. Microwave and Optical Technology Letters. 2009;**51**(2):411-413

[12] Mezaal YS, Eyyuboglu HT, Ali JK. New microstrip bandpass filter designs based on stepped impedance Hilbert fractal resonators. IETE Journal of Research. 2014;**60**(3):257-264

[13] Mezaal YS, Ali JK, Eyyuboglu HT. Miniaturised microstrip bandpass filters based on Moore fractal geometry. International Journal of Electronics. 2015;**102**(8):1306-1319

[14] Ali JK, Miz'el YS. A new miniature Peano fractal-based bandpass filter design with 2nd harmonic suppression. In: Proceedings of 3rd IEEE International Symposium on Microwave, Antenna, Propagation and EMC Technologies for Wireless Communications; Beijing, China; 2009. pp. 1019-1022

[15] Ali JK, Mezaal YS. A new miniature narrowband microstrip bandpass filter

design based on Peano fractal geometry. Iraqi Journal of Applied Physics. 2009;**5**(4):3-9

[16] Ali JK, Alsaedi H, Hasan MF, Hammas HA. A Peano fractal-based dual-mode microstrip bandpass filters for wireless communication systems. In: Proceedings of Progress in Electromagnetics Research Symposium, PIERS; Moscow, Russia; 2012. pp. 888-892

[17] Mezaal YS, Eyyuboglu HT, Ali JK. A new design of dual band microstrip bandpass filter based on Peano fractal geometry: Design and simulation results. In: Proceedings of the 13th IEEE Mediterranean Microwave Symposium, MMS'2013; Saida, Lebanon; 2013. pp. 1-4

[18] Ali JK. A new miniaturized fractal bandpass filter based on dual-mode microstrip square ring resonator. In: Proceedings of the 5th International Multi-Conference on Signals, Systems and Devices, IEEE SSD '08; Amman, Jordan; 2008. pp. 1-5

[19] Ali JK, Hussain NN. A new fractal microstrip bandpass filter design based on dual-mode square ring resonator for wireless communication systems. Iraqi Journal of Applied Physics. 2009;**5**(1):7-14

[20] Ali JK, Hussain NN. An extra reduced size dual-mode bandpass filter for wireless communication systems. In: Proceedings of Progress in Electromagnetics Research Symposium, PIERS 2011; Suzhou, China; 2011. pp. 1467-1470

[21] Liu JC, Liu HH, Yeh KD, Liu CY, Zeng BH, Chen CC. Miniaturized dual-mode resonators with Minkowski-island-based fractal patch for WLAN dual-band systems. Progress in Electromagnetics Research C. 2012;**26**:229-243

[22] Lalbakhsh A, Neyestanak AAL, Naser-Moghaddasi M. Microstrip hairpin bandpass filter using modified Minkowski fractal-shape for suppression of second harmonic. IEICE Transactions on Electronics. 2012;**E95C**(3):378-381

[23] Chen J, Weng ZB, Jiao YC, Zhang FS. Lowpass filter design of Hilbert curve ring defected ground structure. Progress in Electromagnetics Research. 2007;**70**:269-280

[24] Liu HW, Li ZF, Sun XW. A novel fractal defected ground structure and its application to the low-pass filter. Microwave and Optical Technology Letters. 2003;**39**:453-456

[25] Alqaisy M, Chakrabraty C, Ali JK, Alhawari ARH. A miniature fractal-based dual-mode dual-band microstrip bandpass filter design. International Journal of Microwave and Wireless Technologies. 2015;**7**:127-133

[26] Li TP, Wang GM, Lu K, Xu HX, Liao ZH, Zong B. Novel bandpass filter based on CSRR using Koch fractal curve. Progress in Electromagnetics Research Letters. 2012;**28**:121-128

[27] Boutejdar A, Ibrahim AA, Burte EP. DGS resonators form compact filters. Microwaves and RF. 2015;**54**(3):52-60

[28] Boutejdar A, Elsherbini A, Balalem A, Machac J, Omar A. Design of new DGS hairpin microstrip bandpass filter using coupling matrix method. In: Proceedings of Progress in Electromagnetics Research Symposium, PIERS 2007; Prague, Czech Republic; 2007. pp. 261-265

[29] Falconer K. Fractal Geometry: Mathematical Foundations and Applications. Wiley & Sons, West Sussex, England; 2004

[30] Ziboon HT, Ali JK. Minkowski fractal geometry: An attractive choice of compact antenna and filter designs. ARPN Journal of Engineering and Applied Sciences. Accepted, 2018

[31] Ali JK, Ziboon HT. Design of compact bandpass filters based on fractal defected ground structure (DGS) resonators. Indian Journal of Science and Technology. 2016;**9**(39):1-9. DOI: 10.17485/ijst/2016/v9i39/91350

[32] IE3D User's Manual, Release 12.3. Fremont, CA: Zeland Software, Inc.; 2007

[33] Hong JS. Microstrip Filters for RF/Microwave Application. New York: Wiley; 2001

[34] Wang J, Xu LJ, Zhao S, Guo YX, Wu W. Compact quasi-elliptic microstrip lowpass filter with wide stopband. Electronics Letters. 2010;**46**(20):1384-1385

[35] Li JL, Qu SW, Xue Q. Compact microstrip lowpass filter with sharp roll-off and wide stop-band. Electronics Letters. 2009;**45**(2):110-111

[36] Hayati M, Naderi S, Jafari F. Compact microstrip lowpass filter with sharp roll-off using radial resonator. Electronics Letters. 2014;**50**(10):761-762